Preparation and hydration properties of sodium silicate-activated municipal solid waste incineration bottom ash composite slag cementitious materials

Juan Deng *, Guoxiong Wu *, Yuchao Xia , Li Liu

Posted Date: 17 April 2024

doi: 10.20944/preprints202404.1085.v1

Keywords: MSWIBA, sodium silicate-activated, hydration properties, equivalent age modeling

 doi:10.20944/preprints202404.1085.v1

Article

Preparation and Hydration Properties of Sodium Silicate-Activated Municipal Solid Waste Incineration Bottom Ash Composite Slag Cementitious Materials

Juan Deng [1,*], Guoxiong Wu [1,2,*], Yuchao Xia [1] and Li Liu [3]

[1] School of Civil Engineering, Chongqing Jiaotong University, Chongqing 400074, China
[2] Department of Transportation and Municipal Engineering, Chongqing, Jianzhu College, Chongqing 400072, China
[3] School of He Hai, Chongqing Jiaotong University, Chongqing, 400074, China
* Correspondence: 291363739@qq.com; wgx_ph.d@163.com

Abstract: The production of municipal solid waste incineration bottom ash (MSWIBA) is very massive and has the potential to replace cement despite the problems of complex composition, uneven particle size distribution, and low reactivity. This paper adopts sodium silicate activation of MSWIBA-slag to improve the reactivity to prepare composite cementitious materials. It explores the hydration performance study of the composite cementitious materials by isothermal calorimetric analysis, Fourier Transform Infrared (FTIR) spectroscopy, XRD physical diffraction analysis, and SEM/EDS tests. SEM/EDS tests will be used to explore the hydration properties of the composite gelling. The results showed that with the increase of MSWIBA doping, the porosity between the materials increased, the degree of Hydration decreased, and the compressive strength decreased with the rise of MSWIBA. When sodium silicate increased from 25% to 35%, too much alkaline material occurred over the alkaline effect, which inhibited the Hydration of the particles, and the degree of hydration reaction decreased, and the compressive strength decreased accordingly; the exothermic process of Hydration can be mainly divided into five stages, quartz and calcite did not participate in the hydration reaction completely, and sexual aluminum participated in the hydration reaction. The vibrational peaks of Si-O-Ti (T = Si and Al) were present in the material. The vibrational peaks of XRD, FTIR, and SEM-EDS all indicate the presence of silica-aluminate network structures in the hydration products, mainly N-A-S-H and C-A-S-H gels.

Keywords: MSWIBA; sodium silicate-activated; hydration properties; equivalent age modeling

1. Introduction

Solid waste production is enormous, and many countries face serious municipal solid waste (MSW) and environmental pollution. Selecting high-temperature incineration to treat MSW is the most effective way to reduce the amount of volume [1,2]; in general, MSW incineration treatment can reduce its mass by 70% and its volume by 90% [2,3], the rate of unburned ash of the ash residue is 0.7%-2%. The residual rate of the generation of MSWIBA and fly ash of the MSW incineration is about 20% and 2%[4], respectively. Even after incineration, a large amount of MSW incineration bottom ash (MSWIBA) is still generated.

Ordinary silicate cement (OPC) has been widely used in construction. The energy consumption in its production process is an integral part of the energy consumption in the construction industry[5]. As the most consumed type of cement globally, its production process accounts for about 8-10% of anthropogenic CO2 emissions[6]. In addition, cement clinker production requires large amounts of non-renewable resources such as limestone, clay, and coal, which makes the production of OPC

 doi:10.20944/preprints202404.1085.v1

inconsistent with the principles of sustainable development[7]. Several studies have shown that MSWIBA is potentially chemically active and can be blended with slag as a potential replacement material for cement through the action of alkali exciters[8].

Numerous scholars have explored the effect of MSWIBA at different blending levels on cement mortar or cement and found that bottom slag reduces slump value[9,10]. In contrast, the opposite trend was observed when used as a cement substitute. The 28-day compressive strength of the latter was similar to or slightly higher than that of the control mixture (without the addition of MSWIBA) [11,12]. Lin et al. prepared cubic specimens to test the compressive strength of hardened slurries of cementitious materials made from slag and cement by melting MSWIBA into slag and grinding it into powder. The results showed that the 28-day compressive strength of the specimens was 84%~90% of ordinary cement specimens, and the 90-day compressive strength was 95%~110% of ordinary cement specimens [11,13,14]. The effect of Al_2O_3 on MSWIBA by melting the mixture into slag and pulverizing it to replace part of the cement has some strength[11,15].

MSWIBA is characterized by an unstable source, complex composition, non-uniform particle size distribution, and low reactivity, so it is necessary to adopt an activation treatment method for MSWIBA to solve the difficulties and problems of MSWIBA in engineering utilization[9]. Alkali excitation technology uses alkaline exciters to activate the potential activity in MSWIBA and convert them into materials with gelling properties[16]. MSWIBA includes a large number of active components, such as silicon and aluminum, which have the potential to be alkali-activated[14]. Alkali-activated cementitious materials are inorganic compounds made by alkaline excitant activation at temperatures lower than 100°C, which can be extracted from raw materials that are rich in aluminosilicates. This material can be prepared using industrial by-products with potential alkali activation activity as raw materials; the material undergoes Hydration during the alkali activation process, the most critical chemical reaction being that between the aluminosilicate powder and the alkali exciter to produce a hardened slurry with strength[14,16]. According to Davidovits, the resulting geopolymer network consists of SiO4 tetrahedra with oxygen atoms attached and AlO_4 tetrahedra with oxygen atoms attached; the negative charges are balanced by positive ions (e.g., K^+, Na^+, Ca^{2+}, and Li^+) in the cavity framework[16,17].

Compared with slag, MSWIBA has a relatively stable (crystalline) chemical structure and low reactivity in contact with water. When used as cementitious materials, it needs to be activated to improve its properties, of which the most common activation treatments are physical milling activation treatment and activation treatment by alkaline substances[18].

It is proposed that for alkali-activated slag cementitious materials, the effect of using water glass and the strength of the material is more promoted than the use of NaOH [19]; hydroxide ions act as catalysts to promote the reaction to continue, and hydrophilic gel is also involved in the response because water glass contains sodium hydro silicate, which is hydrolyzed to generate sodium hydroxide, and sodium hydro silicate, which includes hydrophilic gel[19].

In summary, the production of MSWIBA is very massive and has the potential to replace cement, exists the problems of complex composition, uneven particle size distribution, and low reactivity; in order to improve the reactivity, in this paper, we used sodium silicate activation of MSWIBA-slag to prepare composite cementitious materials, and through isothermal calorimetric analysis, Fourier transform infrared (FTIR) spectroscopy, XRD physical phase diffraction analysis and SEM and other tests to explore the hydration properties of composite cementation research, in order to promote the harmless disposal of MSWIBA and waste reuse, to reduce the amount of cement, to achieve energy saving and emission reduction to promote the comprehensive reuse of MSWIBA of this solid waste, and to provide theoretical references for the treatment of MSWIBA and application of reference.

2. Experiment

2.1. Experimental Materials

2.1.1. MSWIBA

 doi:10.20944/preprints202404.1085.v1

MSWIBA generated by Chongqing Tongxing waste incineration company which the German Martin SITY2000 reverse thrust tilting grate technology to burn the MSW in the Chongqing area and the residue obtained. After incineration, the ferrous metal is washed, magnetically selected, and then crushed by a crusher after natural drying in the stockpile plant.

It was processed in a muffle furnace at a high temperature of 1000°C for three hours and then ground by a planetary ball mill for 30 min to improve its reactivity. The treated bottom residue of municipal waste incineration was tested by the BET method to obtain a specific surface area of 1.705 m^2g^{-1} and an average pore size of 3.388 nm. The particle size distribution of the period analyzed by the laser particle sizing instrument is shown in Figure 1.

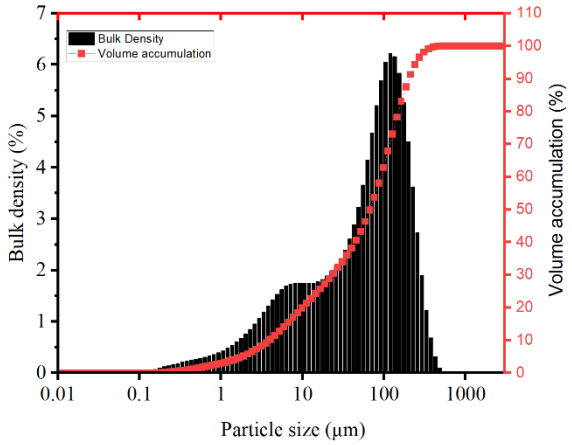

Figure 1. particle size distribution.

Using an X-ray fluorescence spectrometer on MSWIBA and slag, XRF test analysis determines the chemical composition of MSWIBA, as shown in Table 1. According to the definition of Granulated Blast Furnace Slag for Cement (GB/T203-2008), the alkalinity index of MSWIBA is alkalinity index (Mo=(CaO+MgO)/(SiO2+AL2O3)) is about 0.68. According to the definition of Granulated Blast Furnace Slag Used in Cement (GB/T203-2008), Mo<1 is acidic slag.

Table 1. The main chemical composition of MSWIBA and slag（wt%）.

oxides	SiO2	CaO	Al2O3	Fe2O3	P2O5	Na2O	MgO	SO3	K2O
MSWIBA	37.79	28.60	9.34	5.94	5.22	3.25	2.74	2.33	1.52
Slag	30.49	40.83	15.26	0.32	0.02	0.49	8.50	2.08	0.45

2.1.2. Other Materials

The sodium silicate used in this test is pure sodium silicate water glass for analytically pure sodium hydroxide solid S95 slag, China ISO standard sand, isothermal calorimetry experiments using pure water, and other tap water tests.

2.2. Experimental Methods

2.2.1. Material Mixing

According to the results of the previous experiments, five groups of mixing ratios were selected for comparative analysis, as shown in Table 2.; according to the total amount of MSWIBA, slag, sodium silicate alkali component content of the amount of water added, the water-cement ratio (W/B) was fixed at 0.50 for the preparation of slurry. The MSWIBA content was the lowest in the B5S25 experimental group; B29S25, B2, and B29S35 experimental groups had the highest content, followed by B17S25; the sodium silicate content was the highest in the B29S35 experimental group, followed by B5S25 and B29S15 had the lowest content.

 doi:10.20944/preprints202404.1085.v1

Table 2. Detailed mix proportions of the cementitious materials (wt%.

Number	MSWIBA	sodium silicate	Slag	W/C
B5S25	5	25	70	0.5
B29S25	29	25	46	0.5
B17S25	17	25	58	0.5
B29S15	29	15	56	0.5
B29S35	29	35	36	0.5

2.2.2. Experimental Methods

1. Compressive strength

According to the Test Procedure for Cement and Concrete in Highway Engineering and Test Method for Strength of Cementitious Sand (ISO Method) (GB/T17671-2021), the compressive and flexural strength of cementitious sand is determined by molding, the size of the steel-plastic specimen is by the requirements of JC/T726, and the inner length of the test specimen is 40 mm × 40 mm × 160 mm. The specimen and the test specimen are cured in the standard curing room for 20 to 23 hours. After 20 to 23 hours of curing, the specimen is demolded with a machine. After demolding, the compressive and flexural strengths of the specimens were tested according to the curing requirements until the specified age. According to the molding specification, when maintained in the standard maintenance room to 3d and 28d age, different alkali excitation ratios of MSWIBA composite cementitious cemented sand specimens were measured.

2. Isothermal calorimetry experiment

The heat of Hydration of the composite slurry was determined using a TAM Air isothermal calorimeter produced by TA Instruments, Inc. in the United States. The test time was 7d, the calorimeter temperature was 20°C, the water-cement ratio (W/B) was 0.5, and the material composition was consistent with Table 2. Before the experiment, the slurry was thoroughly mixed and poured into the isothermal calorimeter. After exothermic stabilization (30 min), the experimental results were recorded.

3. Hydration product analysis

The net slurry was prepared according to the Chinese national standard (GB/T1346-2011). All the powdered materials (i.e., slag and alkali components) were mixed, and then water was continuously stirred until a homogeneous slurry was formed. The AASC slurry was hydrated at 20±2°C and 95±5 RH for three days 7d, 28d. The AASC samples were then pulverized into small pieces and soaked in anhydrous ethanol for three days to stop the Hydration.

It was dried in an oven at 55°C for 48h, crushed to take some small pieces, and vacuum processed. The microscopic morphology of the different materials was observed by scanning electron microscope. Elemental analysis was carried out with a scanning electron microscope with an energy spectrometer. Some of the small pieces were crushed and milled for 15 min to 20 min and passed through a 200 mesh square hole sieve to carry out the XRD and FTIR spectroscopy tests.

3. Results and Discussion

3.1. Mechanical Properties

3.1.1. Mechanical Properties of Different MSWIBA Doping Levels

Figure 2. shows the compressive strength of the materials with different dosing ratios. The changes in compressive strength are evident. Before the reaction, the compressive strength at 3d is approximately half that at 28d. During the third reaction stage, a significant quantity of unreacted silicate mineral particles exists in the material, which means that with the increase of hydration reaction time, the degree of hydration reaction increases, and compressive strength improves. In the experimental group B5S25, the 3d and 28d compressive strengths were 47.4 Mpa and 70.8 Mpa, respectively, with the highest compressive strengths. Compared with B29S25 and B17S25, with 17%

 doi:10.20944/preprints202404.1085.v1

and 29% MSWIBA, the 3d and 28d compressive strengths show decreasing tendencies with the increase of MSWIBA, and the 3d compressive strengths reduce by 26.6% and 26.8%, respectively. The 28d compressive strengths decrease by 11.0% and 16.5%. It shows that with the increase of MSWIBA, many MSWIBA particles in the early stage of Hydration of the unreacted particles increased, with the porosity between the material decreased. Hydration decreases, and the compressive strength decreases with the increase of MSWIBA.

3.1.2. Mechanical Properties of Different Sodium Silicate Dosages

Figure 2. shows that the 3d and 28d compressive strengths of 15% sodium silicate and 29% MSWIBA experimental group B29S15 were 34.3 Mpa and 52.5 Mpa, respectively. The 3d and 28d compressive strengths of the B29S25 were the highest compared with B29S15 and B29S35, which were increased by 1.2% and 12.6% compared to B29S15. The compressive strengths of the B29S35 experimental group were the lowest, only 8.8 Mpa and 17.3 Mpa, 74.3% and 67.0% lower than B29S25, respectively. It means that while sodium silicate increases from 15% to 25%, the alkaline material increases, making the Hydration of sodium silicate particles in the alkaline environment increase, the degree of hydration reaction increases, the porosity decreases and promotes the generation of hardened slurry with strength, and the compressive strength increases. When the sodium silicate rises from 25% to 35%, the alkaline material is too much over-alkaline, which inhibits the Hydration of particles, the degree of hydration reaction decreases, and the compressive strength decreases.

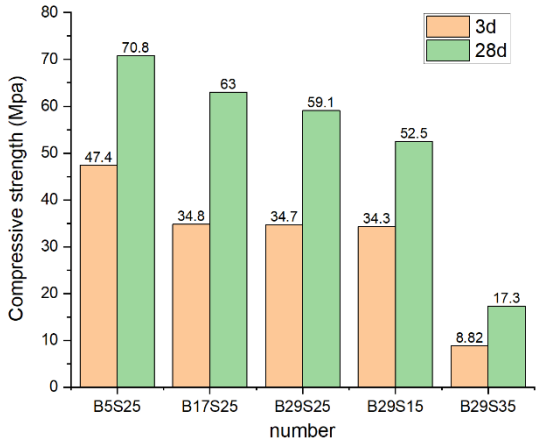

Figure 2. Compressive strength of MSWIBA slag composite cementitious material activated by sodium silicate.

3.2. Hydration Process

3.3.1. Heat of Hydration

Figure 3 shows the calorimetric response and the exothermic process measured using isothermal calorimeter tests, summarized as follows.

Roughly divided the hydration process into five phases: an initial induction phase, an induction phase, an acceleration phase, a deceleration phase, and a steady state phase[20]. The materials do not have an apparent initial induction or induction period, and there is a prominent exothermic peak at the beginning of Hydration.

The first stage is the initial induction period; the initial stage is a transient state in which the mixed slag dissolves rapidly. At this time, the aluminum silicate precursor gradually dissolves and destroys, forming an unstable iso-phase[20,21].

The second phase is the induction phase, which proceeds from the initial induction phase. At this point, Ca2+ in the cementitious materials dissolves with the alkali activator, causing the ionic

 doi:10.20944/preprints202404.1085.v1

concentration mixing solution to be too high and the dissolution of the aluminosilicates to be inhibited[20].

The third, accelerated phase, ranges from 10 mins to 2-3 h; at this time, with the dissolution of the alkali activator, the concentration of OH- in the solution increases, and the activity of the MSWIBA and slag is activated, under which hydration and polymerization reactions take place to produce gel products such as (N)C-A-S-H.

The fourth is deceleration, ranging from 2~3h and 24h; at this time, the hydration rate starts to slow down with the increase of hydration products because the surface of MSWIBA and slag particles gradually covered by the hydration products, which reduces the contact area[20]. This phase is called the deceleration phase.

Stage 5: Steady state stage, over 24 hours. The hydration rate was relatively low and stable, called the stabilization period. At this time, the cementitious material gradually hardens from the paste, the hydration reaction forms a hardened slurry, and the pore structure is formed stably[20].

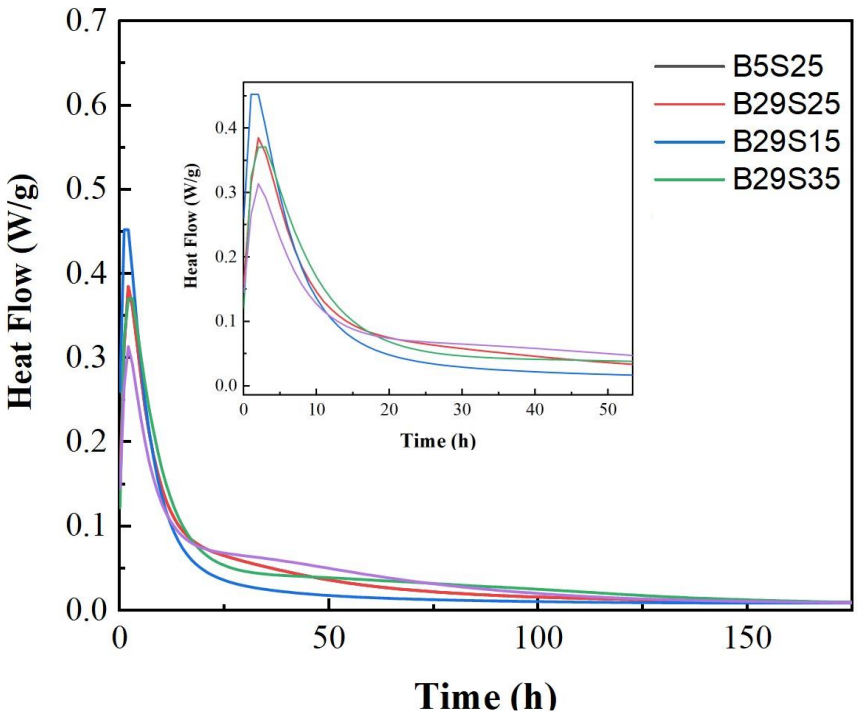

Figure 3. Hydration heat release rate diagram.

3.3.2. Hydration Exothermic Equivalent Age Modeling

The heat of Hydration was expressed using hyperbolic form[22], as shown in the following equation (3.1):

$$Q(t) = Q_{\max} t / (n + t) \tag{3.1}$$

Where n is the heat of Hydration at half the age, the above equation can be rewritten in the following form (3.2):

$$\frac{t}{Q(t)} = \frac{n}{Q_{max}} + \frac{t}{Q_{max}} \tag{3.2}$$

Firstly, choose the ratio t/Q(t) as the vertical coordinate and t as the horizontal coordinate for a graph. Then, a fitting analysis was performed to obtain the slope of the line as 1/Qmax and the line intercept in the vertical coordinate as n/Qmax, leading to the value of n. This critical parameter helps us accurately describe the Hydraulic exothermic process.

 doi:10.20944/preprints202404.1085.v1

The equations can be obtained by calculation using Qmax. Figure 4. shows the Hydration and heat release models of the B5 and B6, as shown in Equation 2 and Equation 3, respectively.

$$Q(t) = \frac{10000t}{86.2 + 6.00089t} \tag{3.3}$$

$$Q(t) = \frac{10000t}{90.8 + 5.85017t} \tag{3.4}$$

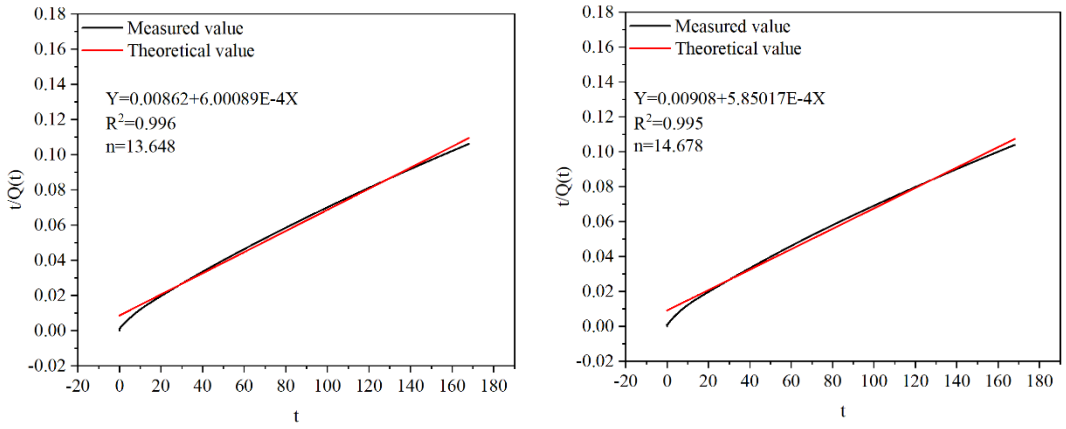

Figure 4. Model parameter-solving diagrams.

Figure 5. illustrates the cumulative heat release of the material, as predicted by the hydration heat release model, alongside the accumulated heat release measured through testing. It can be seen from the figure that with the increase of MSWIBA content, both the total amount of accumulated heat release is reduced, and the theoretical value is less than the test value during the heat release. The difference does not change much in the 60 hours before the heat release of hydration. After 72h, the difference increases with time, and the fitting degree is not good in the late stage of hydration heat release.

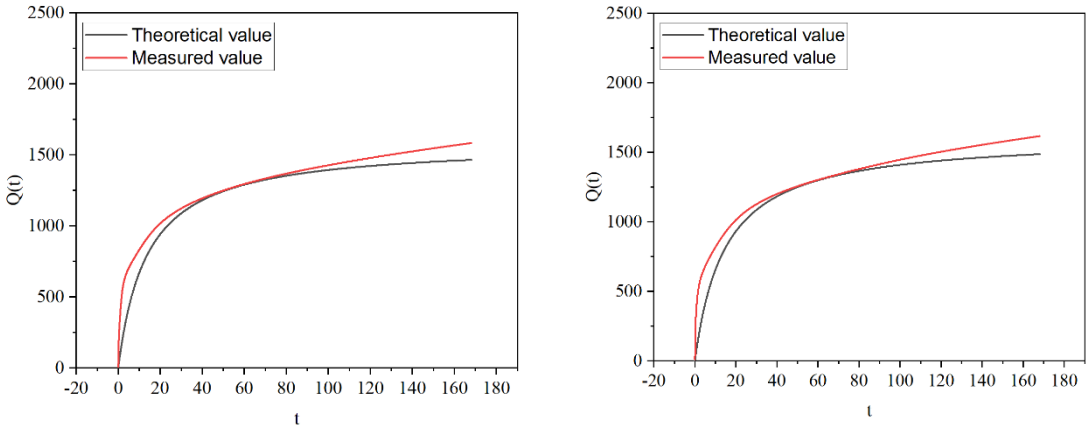

Figure 5. Comparison between the theoretical and measured values.

3.3. Hydration Products and Hydration Properties

3.2.1. XRD

Figure 6. compares the ratios of the three materials after 3 and 28 days of B5S25 curing. Compared with the XRD test curves of the raw materials, the X-ray diffraction peaks of alkali-excited

 doi:10.20944/preprints202404.1085.v1

MSWIBA are relatively small in angle, indicating the formation of a new amorphous gel[23]. The broader diffraction peaks were mainly associated with the amorphous material of the feedstock and the newly formed amorphous gels of the reaction products.

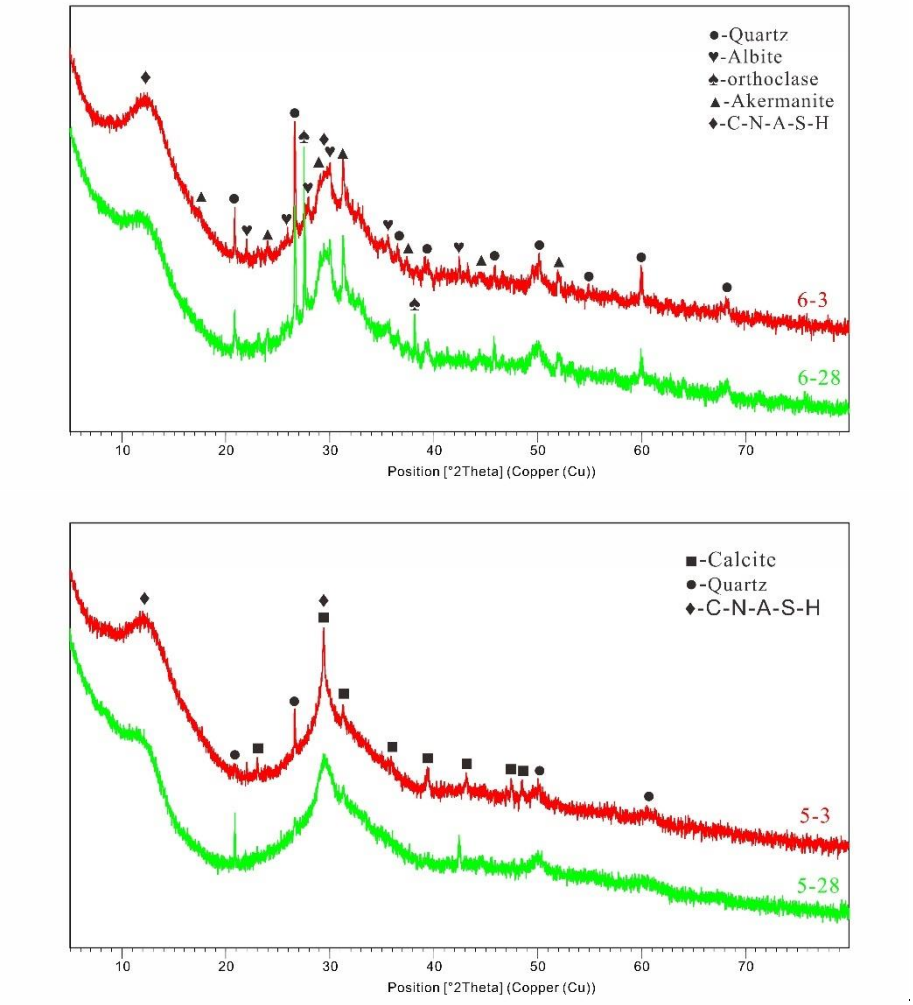

Figure 6. (a)(b) XRD patterns of B5S25 and B29S25.

By XRD analysis, it is difficult to identify and differentiate the amorphous N-A-S-H and C-A-S-H gels. Quartz and mullite crystals in MSWIBA were not fully involved in the reaction during the hydration process. They have distinct diffraction peaks in the XRD patterns.

In contrast, the difference between specimen peaks is relatively tiny at three days, indicating that adding MSWIBA weakens the early Hydration of alkali-stimulated composite collodion materials[23]. In addition, the trend is from high to low, which is consistent with the results of the mechanical properties of the slurry. A comparison of the plots of specimen B5S25 showed that the amount of hydration products increased with the age of Hydration[23]. XRD plots of group B29S25 showed changes in the physical phases after 3 and 28 days of curing. The content of MSWIBA increased from 5% to 29%, and the physical phases of the main hydration products in the gelling system were similar. However, an increase in the diffraction peaks of the new and firmer phases was found.

In conclusion, the physical phases of quartz and calcite were in the XRD patterns of the two sets of diagrams. As the hydration process proceeds, quartz and calcite decrease, suggesting that these two substances transform into different substances during the hydration process. The reduction of quartz and calcite indicates that these two substances are involved in the hydration reaction, and the primary substances of the hydration reaction are similar. The C-A-S-H peaks of the 28d groups are higher than the corresponding positions of the 7d peaks, which indicates that the degree of hydration reaction is higher.

 doi:10.20944/preprints202404.1085.v1

3.2.2. Fourier Transform Infrared (FT-IR) Analysis

Fourier transform infrared spectroscopy (FT-IR) was used to obtain the structural characteristics. Figure 7. shows the structure of the functional groups of B5S25. As shown, there is an O-H telescopic vibrational absorption peak at 3464 cm^{-1}, generated by the telescopic vibration of H-O-H in water[18]. There is an O-H bending vibration peak at 1651 cm^{-1}, generated by the bending vibration of O-H in water. These peaks can indicate the amount of chemically bound water in alkali-activated MSWIBA slag binder. The higher intensity of the peaks indicates the presence of more chemically bound water in the binder[21]; moreover, no distinct and sharp bands associated with the stretching vibration of the OH single bond in Ca(OH)2 were observed at 3644 cm^{-1}, whereas the presence of the absorption band material of the Al(Mg)Si-OH phase was seen in the infrared spectral map of MSWIBA at 3620 cm^{-1}, which indicates that the Aluminosilicate in MSWIBA actively participates in the hydration reaction process during alkali activation production, thus eliminating the vibrations of Al(Mg)Si-OH[18,24]. This suggests that the alkaline chemical environment plays a crucial role in reducing the crystallinity of quartz in MSWIBA and domestic waste incineration slag.

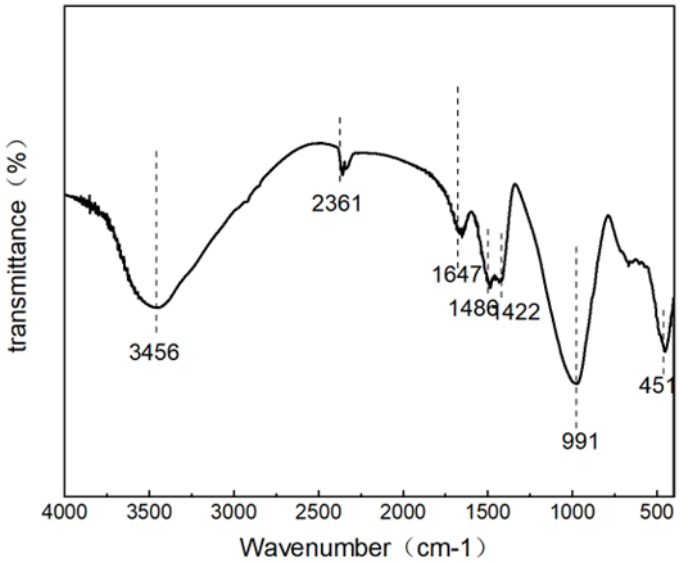

Figure 7. FTIR spectrum of B5S25.

1420 cm^{-1} is the absorption peak of the C-C stretching vibration caused by the symmetric stretching vibration of CO_3^{2-}.3464 cm^{-1} annexes a broad water peak and not low intensity, which indicates that the water occupies a certain proportion of the sample, suggesting that the binder contains a higher amount of chemically binding water. In the range of 600 to 1200 cm^{-1}, the vibrational peaks with Si-O-Ti (T=Si and Al) exist, indicating that the silicoaluminate network structure exists in all the hydration products; this suggests that the alumino-silicates in the bottom slag of the domestic waste incineration actively participate in the hydration reaction process of the bottom slag of the domestic waste incineration slag in the alkaline activation of the production process. The results show that the samples are present in the C-A-S-H and Calcium alumina This is consistent with the X-ray diffraction and SEM-EDS analysis results.

3.2.3. Scanning Electron Microscope

According to previous results, amorphous gels usually consist of C-A-S-H and N-A-S-H gels coexisting in alkali-activated slag/systems, and analyses showed the presence of N-A-S-H gels, C-(A)-S-H gels, and some unreacted MSWIBA and slag particles. These components showed a disordered lattice structure and showed excellent compatibility[18,25,26], indicating that the content of sodium silicate has a significant influence on the surface morphology and structure of the composite gelling material.

 doi:10.20944/preprints202404.1085.v1

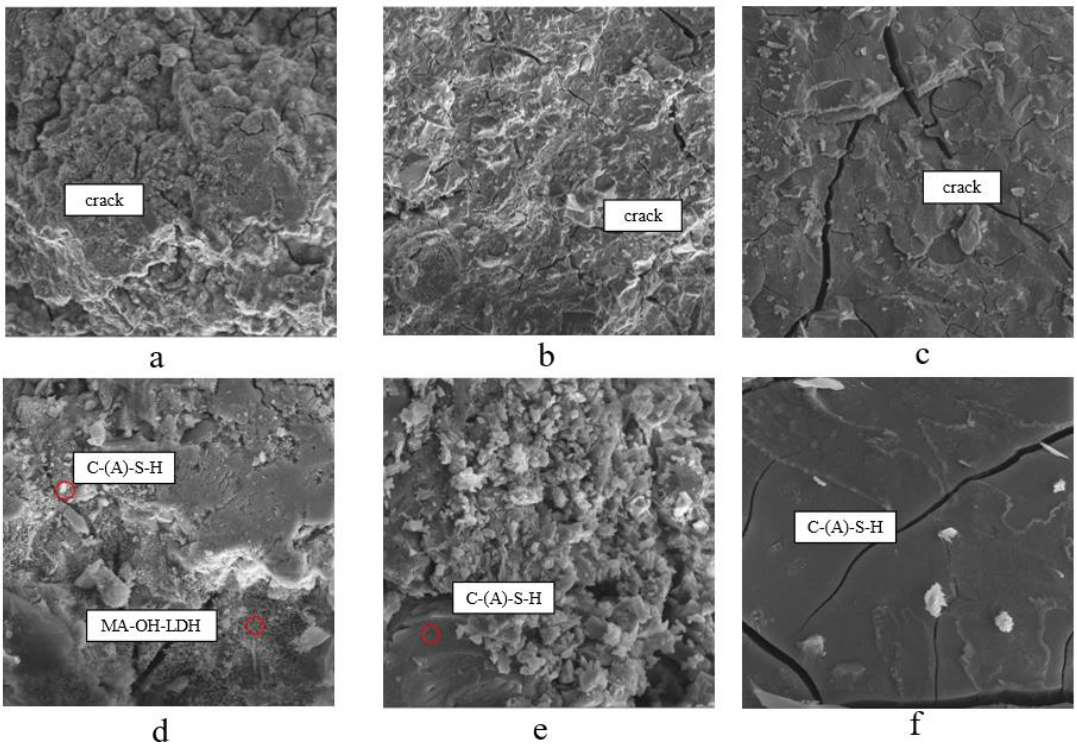

Figure 8. SEM observation of B29S15,B29S35 and B29S25 at 28 d.

As can be seen from Figure 7(a)(b)(c), the samples in groups B29S15, B29S35, and B29S25 have multiple microcracks due to drying shrinkage. Among them, the width and number of microcracks on the surface of B29S35 samples were significantly higher than that of B29S15, and there were few microcracks in B29S25. This is because when the alkali exciter dosage is 15%, it cannot provide enough alkaline material, the activity of the gelling system is insufficient, and the particles can not react sufficiently, with lower strength, showing a loose micro-morphology, which indicates that there are many unhydrated particles. With the alkali exciter content increased to 25%, the activity of the gelling system is enhanced, which promotes the hydration reaction effect, making the particles fully dissolved and hydrated; from the Figure, we can see that the micrograph of the B29S25 specimen shows dense characteristics, and the hydration reaction products are tightly wrapped around the un-reacted substrate particles; at the same time, the substrate is well compacted, and no apparent micro-cracks were found, which makes the hardened slurry compressive properties show excellent performance. When the alkali exciter dosing over 25% to 35%, the alkali exciter was in excess, which inhibited the occurrence of the hydration reaction, and a large number of particles were exposed, which were not sufficiently hydrated to generate sufficient crystalline phase; the loose morphology of B29S35 with a vast number of microcracks can be seen in Figure 7. (b).

Dense amorphous gel phase C-(A)-S-H with large-size silicate particles was found in Figure 7. (d)(e)(f), in which B29S35 had the most and B29S35 the least; in Fig. (e), a network-like gel phase was found, and 35% alkali stimulant dosing of B29S35 contained a large number of unhydrated particles, compared to B29S25 which also had partially exposed and unhydrated particles. The 28d compressive strength of the B29S35 sample is only about one-third of that of B29S25. Many needle-like and rod-like AFt crystals are found in Fig. (f), which enhance the interconnection with the C-A-S-H gel[27].

The results of this study show that the micro-morphological characteristics performance and the compressive strength test results performance is consistent with the alkalinity of the alkali exciter is one of the very important factors in the formation of MSWIBA composite cementitious materials and the final hydration products, with the increase in alkali exciter from 15% to 25%, the rise in alkali exciters significantly promotes the conversion of the free alkali to the bonded alkali, and the

 doi:10.20944/preprints202404.1085.v1

stimulation of the activator is enhanced, which helps the The hydration reaction occurs, more hydrated crystalline phase is generated, and the strength of the cementitious system is improved; when the alkali exciter is increased from 25% to 35%, the alkali exciter dosage is too much, resulting in over-alkali effect, the stimulation ability of the activator is reduced, and the hydration reaction is inhibited, and there are a large number of unhydrated particles, and the microscopic morphology shows that the product is very loose, and the number of microcracks is enormous, and the compressive strength decreases significantly.

4. Conclusion

This research investigated the preparation and the hydration of properties of the sodium silicate activation of MSWIBA-slag composite cementitious materials, which can get conclusions as below shown:

The compressive strength decreases with the increase in MSWIBA. While sodium silicate is below 25%, the compressive strength exhibits an increasing trend with higher silicate levels.; While above 25%, the compressive strength decreases as silicate levels rise.

The hydration process can be divided into five phases: the heat reduces with the increase of MSWIBA, and the hyperbolic form models less than the test value。

As the hydration process proceeds, quartz and calcite decrease, and activated aluminum participates in the hydration reaction. XRD, FTIR, and SEM results showed that there was a silica-aluminate network structure in the hydration products, mainly N-A-S-H and C-A-S-H gels.

Reference

1. R.V. Silva, J. de Brito, C.J. Lynn, R.K. Dhir, Environmental impacts of the use of bottom ashes from municipal solid waste incineration: A review, Resources, Conservation and Recycling 140 (2019) 23-35.
2. R.M. Barros, 4 - Municipal solid waste ash, in: R. Siddique, R. Belarbi (Eds.), Sustainable Concrete Made with Ashes and Dust from Different Sources, Woodhead Publishing2022, pp. 93-177.
3. J.A. Stegemann, J. Schneider, B.W. Baetz, K.L. Murphy, Lysimeter washing of MSW incinerator bottom ash, Waste Management & Research 13(2) (1995) 149-165.
4. J. Liu, Z. Wang, Z. Li, G. Xie, W. Zhang, H. Jin, F. Xing, Investigation of the cyclic separation of dioxins from municipal solid waste incineration fly ash by using fat, Journal of Cleaner Production 450 (2024) 141840.
5. M.B. Ali, R. Saidur, M.S. Hossain, A review on emission analysis in cement industries, Renewable and Sustainable Energy Reviews 15(5) (2011) 2252-2261.
6. J. Wang, Z. Zhai, Y. Jing, C. Zhang, Influence analysis of building types and climate zones on energetic, economic and environmental performances of BCHP systems, Applied Energy 88(9) (2011) 3097-3112.
7. M. González-Torres, L. Pérez-Lombard, J.F. Coronel, I.R. Maestre, D. Yan, A review on buildings energy information: Trends, end-uses, fuels and drivers, Energy Reports 8 (2022) 626-637.
8. X. Gao, B. Yuan, Q.L. Yu, H.J.H. Brouwers, Characterization and application of municipal solid waste incineration (MSWI) bottom ash and waste granite powder in alkali activated slag, Journal of Cleaner Production 164 (2017) 410-419.
9. P. Tang, W. Chen, D. Xuan, Y. Zuo, C.S. Poon, Investigation of cementitious properties of different constituents in municipal solid waste incineration bottom ash as supplementary cementitious materials, Journal of Cleaner Production 258 (2020) 120675.
10. N. Yamaguchi, M. Nagaishi, K. Kisu, Y. Nakamura, K. Ikeda, Preparation of monolithic geopolymer materials from urban waste incineration slags, Journal- Ceramic Society Japan 121(1417) (2013) 847-854.
11. K.L. Lin, D.F. Lin, Hydration characteristics of municipal solid waste incinerator bottom ash slag as a pozzolanic material for use in cement, Cement and Concrete Composites 28(9) (2006) 817-823.
12. C.J. Lynn, R.K. Dhir, G.S. Ghataora, Municipal incinerated bottom ash characteristics and potential for use as aggregate in concrete, Construction and Building Materials 127 (2016) 504-517.
13. R. Pouhet, M. Cyr, Carbonation in the pore solution of metakaolin-based geopolymer, Cement and Concrete Research 88 (2016) 227-235.
14. G.S. Ryu, Y.B. Lee, K.T. Koh, Y.S. Chung, The mechanical properties of fly ash-based geopolymer concrete with alkaline activators, Construction and Building Materials 47 (2013) 409-418.

 doi:10.20944/preprints202404.1085.v1

15. G. Huang, Y. Ji, J. Li, Z. Hou, C. Jin, Use of slaked lime and Portland cement to improve the resistance of MSWI bottom ash-GBFS geopolymer concrete against carbonation, Construction and Building Materials 166 (2018) 290-300.
16. Z. Xiaolong, Z. Shiyu, L. Hui, Z. Yingliang, Disposal of mine tailings via geopolymerization, Journal of Cleaner Production 284 (2021) 124756.
17. J.L. Provis, P. Duxson, J.S.J.V. Deventer, Geopolymer technology and the search for a low-CO2 alternative to concrete, (2007).
18. A. Moussadik, F. Ouzoun, H. Ez-zaki, M. Saadi, A. Diouri, Mineralogical study of a binder based on alkali-activated coal gangue, Materials Today: Proceedings (2023).
19. J.M. Etcheverry, Y.A. Villagran-Zaccardi, P. Van den Heede, V. Hallet, N. De Belie, Effect of sodium sulfate activation on the early age behaviour and microstructure development of hybrid cementitious systems containing Portland cement, and blast furnace slag, Cement and Concrete Composites 141 (2023) 105101.
20. J. Zhao, B. Long, G. Yang, Z. Cheng, Q. Liu, Characteristics of alkali-activated slag powder mixing with seawater: Workability, hydration reaction kinetics and mechanism, Case Studies in Construction Materials 17 (2022) e01381.
21. X. Zhang, W. Wang, Y. Zhang, X. Gu, Research on hydration characteristics of OSR-GGBFS-FA alkali-activated materials, Construction and Building Materials 411 (2024) 134321.
22. Zhu Bofang, Principle and Application of Finite Element Method, 4 ed., China Water Resources and Hydropower Press.
23. G. Huang, K. Yang, Y. Sun, Z. Lu, X. Zhang, L. Zuo, Y. Feng, R. Qian, Y. Qi, Y. Ji, Z. Xu, Influence of NaOH content on the alkali conversion mechanism in MSWI bottom ash alkali-activated mortars, Construction and Building Materials 248 (2020) 118582.
24. A. Mitrović, M. Zdujić, Preparation of pozzolanic addition by mechanical treatment of kaolin clay, International Journal of Mineral Processing 132 (2014) 59-66.
25. B. Li, Z. Liu, Q. Sun, L. Yang, Preparation of alkali-activated nickel slag-based cemented tailings backfill: Workability, strength characteristics, localized deformation and hydration mechanism, Construction and Building Materials 411 (2024) 134639.
26. M.R. Ahmad, L.-P. Qian, Y. Fang, A. Wang, J.-G. Dai, A multiscale study on gel composition of hybrid alkali-activated materials partially utilizing air pollution control residue as an activator, Cement and Concrete Composites 136 (2023) 104856.
27. Chen Shikun, Study on Mechanical properties and Microscopic mechanism of metakaolin base polymer concrete, 2019.